materials

MDPI

Communication

Molten Salt Synthesis of Intermetallic Compound TiNi Nanopowder Passivated by TiO_x Shell Prepared from $NiTiO_3$ for Catalytic Hydrogenation

Yasukazu Kobayashi [1,*], Shota Yokoyama [2] and Ryo Shoji [2]

[1] Renewable Energy Research Centre, National Institute of Advanced Industrial Science and Technology, 2-2-9 Machiikedai, Koriyama 963-0298, Japan
[2] Department of Chemical Science and Engineering, National Institute of Technology, Tokyo College, 1220-2 Kunugida, Hachioji 193-0997, Japan
* Correspondence: yasu-kobayashi@aist.go.jp; Tel.: +81-29-861-4014

Abstract: Titanium-nickel alloy is an attractive material due to its unique properties of shape memory effect, superior elasticity, and biocompatibility. Generally, Ti-Ni alloy powders are prepared from pure elemental powders of Ti and Ni as starting materials, but it is an energy-intensive process to obtain pure titanium. In this study, intermetallic compound TiNi powder passivated by TiO_x shell was prepared by directly reducing a commercial $NiTiO_3$ using CaH_2 reducing agent in a molten LiCl at 650 °C. Analyses by X-ray diffraction, scanning electron microscopy/transmission electron microscopy with energy-dispersive X-ray spectroscopy and X-ray photoelectron spectroscopy revealed that the powder had a core–shell structure, with the core of TiNi and the shell of TiO_x-rich composition with scarce metallic Ni nicely catalyzing hydrogenation reactions with good recyclability and stability.

Keywords: intermetallic compound; TiNi; molten salt synthesis; 4-Nitrophenol hydrogenation

check for updates

Citation: Kobayashi, Y.; Yokoyama, S.; Shoji, R. Molten Salt Synthesis of Intermetallic Compound TiNi Nanopowder Passivated by TiO_x Shell Prepared from $NiTiO_3$ for Catalytic Hydrogenation. *Materials* **2022**, *15*, 8536. https://doi.org/10.3390/ma15238536

Academic Editor: Anna Knaislová

Received: 19 October 2022
Accepted: 28 November 2022
Published: 30 November 2022

1. Introduction

Titanium-nickel alloy is an attractive material because of its unique properties of shape memory effect, superior elasticity, and biocompatibility, as well as corrosion resistance, allowing for various industrial applications in biomedical and structural engineering fields [1–4]. Ti-Ni alloy powders are typically prepared from pure elemental powders of Ti and Ni as starting materials [5–10], where they are melted at a high temperature of ~2000 °C under an inert atmosphere/vacuum for well-mixing. Some advanced methods for preparing finer ones, such as self-propagating high-temperature synthesis (SHS) [11–17], combustion method [18,19], plasma/laser techniques [20–23], and so on, have been reported. It is a relatively energy-intensive process to produce pure titanium, which is used as one of the raw materials to prepare titanium alloys from oxide ores, such as TiO_2 and $FeTiO_3$. Therefore, it would be innovative to prepare titanium alloys directly from titanium oxides. We previously succeeded in preparing intermetallic compound TiFe powders from the oxide precursors, including TiO_2 [24] and $FeTiO_3$ [25] by directly reducing them and then alloying them simultaneously in highly reductive conditions of molten LiCl-CaH_2 at 600 °C. Under these conditions, hydride ions (H^-) or calcium metals that are produced from CaH_2 could as strong reducing agents to readily reduce the titanium oxide precursors at such a low temperature.

In this study, intermetallic compound TiNi powder was prepared by directly reducing a commercial $NiTiO_3$ in molten LiCl-CaH_2 at 650 °C. Molten salt synthesis is a good technique to obtain intermetallic compounds available for catalyst application [26]. The $NiTiO_3$ precursor had a high crystallinity, indicating that Ni and Ti had previously mixed well on an atomic level, resulting in the formation of homogeneous TiNi powder by deoxidization. Nickel metals, titanium metals and their alloys are well-known active catalysts for hydrogenations [27–30]. Efficient water purification techniques are highly aspired [31,32]. In this study, the prepared TiNi was used to catalytically hydrogenate *p*-nitrophenol (4-NP) to confirm its potential application as a catalyst available in liquid phase.

2. Materials and Methods

Commercial $NiTiO_3$ (99.9%, Kojundo Chemical Laboratory Co., Ltd., Tokyo, Japan) was used as a precursor to prepare the intermetallic compound TiNi. First, it was mixed in the air with CaH_2 (94.0%, JUNSEI Chem. Co., Ltd., Tokyo, Japan) and LiCl (99.0%, Wako Pure Chem. Corp., Osaka, Japan) in a mortar with a weight ratio of $NiTiO_3/CaH_2$/molten salt source = 2/6/3 [33]. The mixed powder was then loaded into a stainless-steel reactor and heated in argon for 2 h at 650 °C. The reduction temperatures of 650 °C were chosen because the intermetallic TiNi phase is stable above 630 °C [34]. Finally, the reduced precursors were crushed in a mortar and rinsed with a 0.1 M NH_4Cl aqueous solution made with NH_4Cl (99.5%, Wako Pure Chem. Corp.) and distilled water to obtain the final product powder (TiNi).

The crystal structure of the prepared samples was examined using X-ray diffraction (XRD, MiniFlex 600, Rigaku, Tokyo, Japan) with CuK_α radiation at 40 kV and 15 mA. The measurements were ranged from 20° to 130° with a step interval of 0.01° and a scan speed of 10°/min. The porosity was examined using N_2 adsorption at −196 °C (BELLSORP mini-II, MicrotracBEL Corp., Osaka, Japan). The samples were pretreated at 200 °C for 30 min under a vacuum in order to remove the water contained in the samples before the measurement. Scanning electron microscopy (SEM, JSM-7400F, JEOL Ltd., Tokyo, Japan) and transmission electron microscopy (TEM, a Tecnai Osiris, FEI system) were used to examine the morphology, and elemental analysis was performed using energy dispersive X-ray spectrometry (EDX). Cupper-based micro grids (NP-C15 (Lacy Carbon film), Okenshoji Co., Ltd., Tokyo, Japan) were used to fix the sample powder and therefore non-identified signals in the images are mainly due to the cupper. The chemical states and composition of the prepared samples' surface were determined using X-ray photoelectron spectroscopy (XPS) (PHI X-tool, ULVAC-PHI, Inc., Kanagawa, Japan) operated with AlK_α radiation. The chemical shifts were calibrated by fixing C1s peak of the surface carbonaceous contaminants at 284.8 eV.

The catalytic reactions were conducted in 20 mL glass bottles following the previously reported procedures [35]. In the catalytic tests, 1 mL of 4-NP solution (14 mM) was added to a bottle containing 10 mg of catalyst powder, 1 mL of $NaBH_4$ solution (0.42 M), and 7 mL of distilled water as the solvent. To satisfy first-order reaction kinetics, the initial concentration of $NaBH_4$ (0.047 M) was 30 times higher than that of 4-NP (1.6 mM). The reactions were stirred at 50 °C until the concentrations reached zero. An aluminum heat sink mounted on a hotplate was used to maintain a constant solution temperature. A small aliquot (100 μL) solution was taken to determine the concentration changes at reaction times of 0.5–50 min. The conversion of 4-NP to *p*-aminophenol was monitored using an ultraviolet-visible spectrometer using the respective absorbance changes at 401 and 315 nm. $NiTiO_3$ and TiO_2 (JRC-TIO-4 (2) (Degussa P25), supplied by Japan Reference Catalyst Society, 50 m^2/g [36]) were also tested for references.

3. Results and Discussion

3.1. Synthesis of TiNi Nanopowder from $NiTiO_3$

Figure 1 shows the XRD patterns of commercial $NiTiO_3$ and prepared TiNi. The observed peaks were perfectly identified as $NiTiO_3$ and intermetallic compound TiNi with a cubic CsCl-type crystal structure, respectively. The crystallite sizes were calculated using the Sherrer equation with the main peak observed around 42°–43° for the intermetallic TiNi was 72.9 nm. The measured BET surface area using N_2 adsorption was 6.0 m^2/g. These values are summarized in Table 1. A larger crystallite size TiNi with a smaller BET surface area was obtained in this study compared with our previous results of TiFe (46.2–65.2 nm, 13.9–20.0 m^2/g) [24,25]. Because nickel oxides are more easily reduced than iron oxide because of the more thermodynamic stability of FeO than NiO [37], the rate of crystal growth for TiNi crystal particles in the reduction/alloying processes at 650 °C could be accelerated to form the final larger particles.

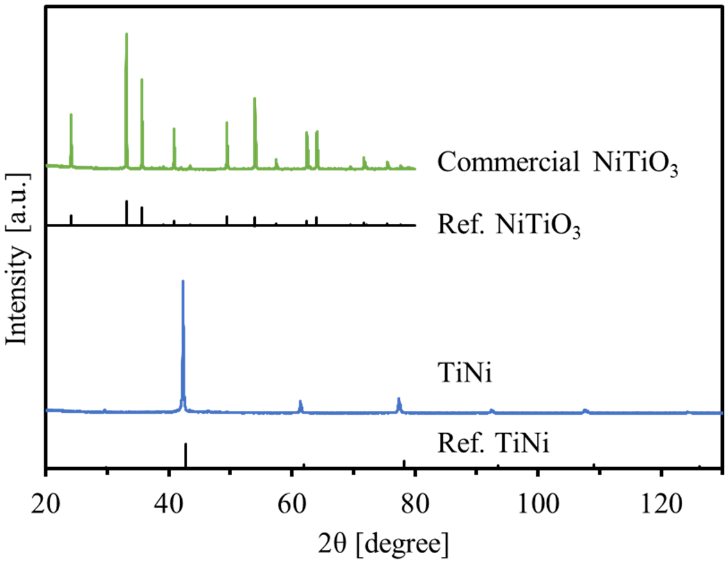

Figure 1. XRD patterns of commercial $NiTiO_3$ and the prepared TiNi.

Table 1. Crystalline sizes, BET surface areas (S.A.), and elemental molar ratios measured by XPS, SEM-EDX, and TEM-EDX.

Sample	Crystalline Size [nm]	BET S.A. [m^2/g]	Method	Elemental Molar Ratio [mol%]		
				Ti	Ni	O
TiNi	72.9	6.0	XPS	23.6	1.1	75.2
				24.3	1.0	74.7
				24.7	2.0	73.3
			SEM-EDX	40.4	42.8	16.8
			TEM-EDX	49.9	47.2	2.9
				49.9	44.4	5.7

Figures 2 and S1 show the SEM images for $NiTiO_3$ and the prepared TiNi, respectively. For $NiTiO_3$, rocky pieces with high crystallinity were observed. Smooth surfaces with microscale morphologies were observed in magnified views. Microscale TiNi pieces were similarly observed, but when examined under high magnification, their porosity was very high in the nanoscale range. In the deoxidization process where oxygen atoms were removed from $NiTiO_3$ to form TiNi, the aggregation of previously oxygen-occupied spaces in the final TiNi could attribute to the formation of the porous structure. Similar nanosized morphologies were also observed in the TiNi powder prepared similarly but at 800 °C (Figure S2), indicating that the fine morphologies in the prepared TiNi may be thermally stable. Elemental analysis by SEM-EDX was also performed on the prepared TiNi (Figure 2). Impurity elements were detected in small amounts except for Ti, Ni, and O. The molar ratio of Ti/Ni/O was 40.4/42.8/16.8 (Table 1). The result confirmed the formation of the intermetallic compound TiNi with a stoichiometric molar ratio of 1 to 1. Note that the oxygen ratio was a little bit high, indicating surface oxidation (which is discussed later). TEM-EDX was used on the prepared TiNi to examine finer morphology with elemental analysis. EDX was used to perform the elemental analyses at two different positions (Figures 3 and S3). The observed elemental molar ratios are summarized in Table 1. Nanoscale particles nearly corresponding to the crystalline size (72.9 nm) as determined by XRD, were observed in the TEM images. The elemental mappings of Ti and Ni overlapped well, and the molar ratios of the intermetallic compound TiNi were almost stoichiometric. These results also demonstrate the successful preparation of the intermetallic compound TiNi by the direct reduction of $NiTiO_3$.

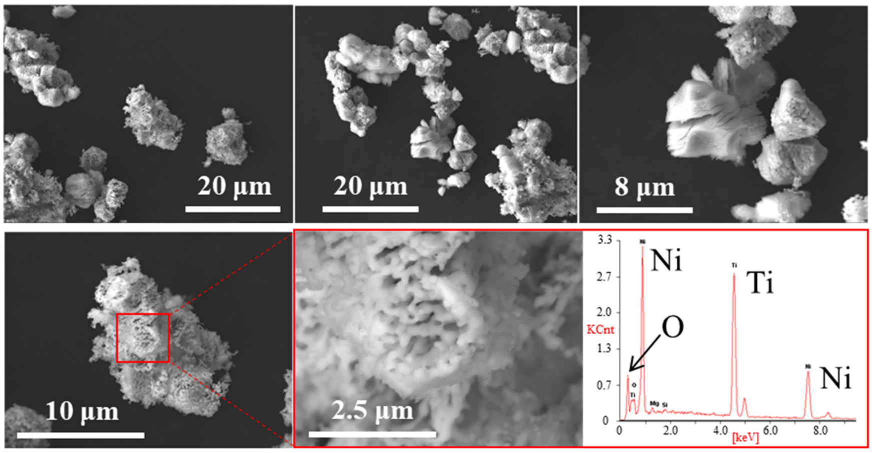

Figure 2. SEM images for the prepared TiNi. EDX spectrum is given at the right-down with Ti/Ni/O = 40.4/42.8/16.8 [mol%].

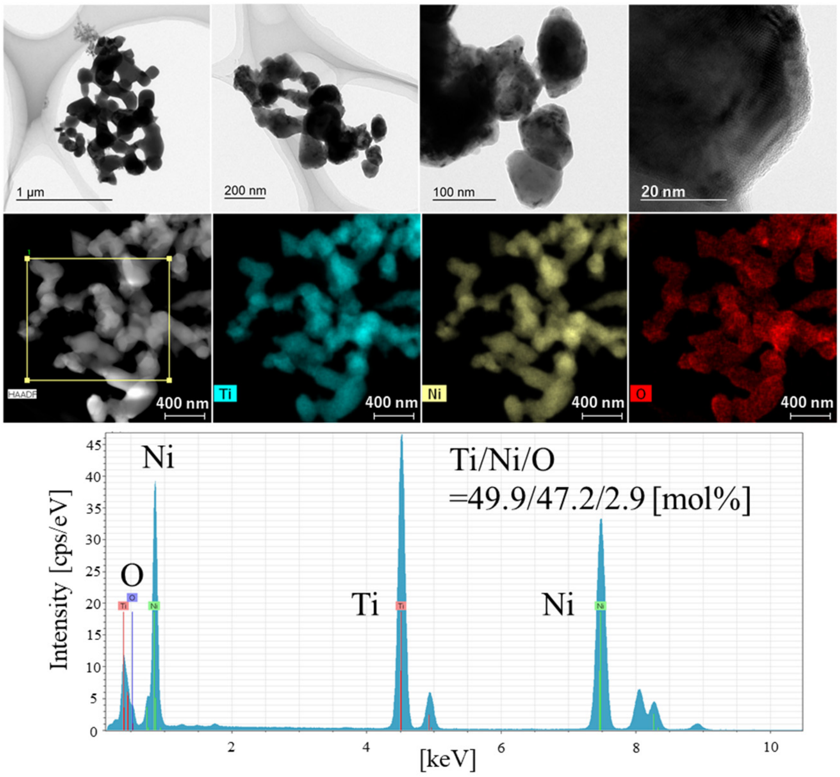

Figure 3. TEM images and the EDX result for the prepared TiNi.

To examine the surface chemical states, XPS measurements were performed on $NiTiO_3$ and the prepared TiNi. The analyses were performed at three different positions for each sample to guarantee the measurement errors. The obtained spectra for C 1s, O 1s, Ti 2p3, and Ni 2p3 orbitals and the molar ratios of Ti/Ni/O are described in Figure 4 and Table 1, respectively. The XPS spectra measured in a wide-scanned mode are shown in Figure S4, where the other elements except Ti, Ni, and O were barely detected. For the O 1s orbital, large signals in a similar degree with $NiTiO_3$ were observed for TiNi. The oxygen ratios determined by XPS were much higher than those determined by SEM-/TEM-EDX (Table 1).

These results indicated that the surface of the prepared TiNi powder was in the form of oxides. For the Ti 2p3 orbital, clear signals assigned to Ti (+4) [38] were observed for both $NiTiO_3$ and TiNi, indicating the formation of TiO_x species on the prepared TiNi surface. For the Ni 2p3 orbital, very small signals assigned to Ni (0) [39] were observed for TiNi, whereas distinct signals to Ni (+2) [39] were observed for $NiTiO_3$. Ti-rich/Ni-deficient surface compositions by XPS for TiNi (Table 1), were extremely different from those by SEM-/TEM-EDX. It was speculated that the prepared TiNi powder has too thin TiO_x surface layers to observe via the employed TEM. Taking the results of XRD, SEM-/TEM-EDX, and XPS together into account, the obtained TiNi possessed a core–shelled structure, such as the core of the intermetallic compound TiNi and the shell of TiO_x-rich composition with a trace of metallic Ni.

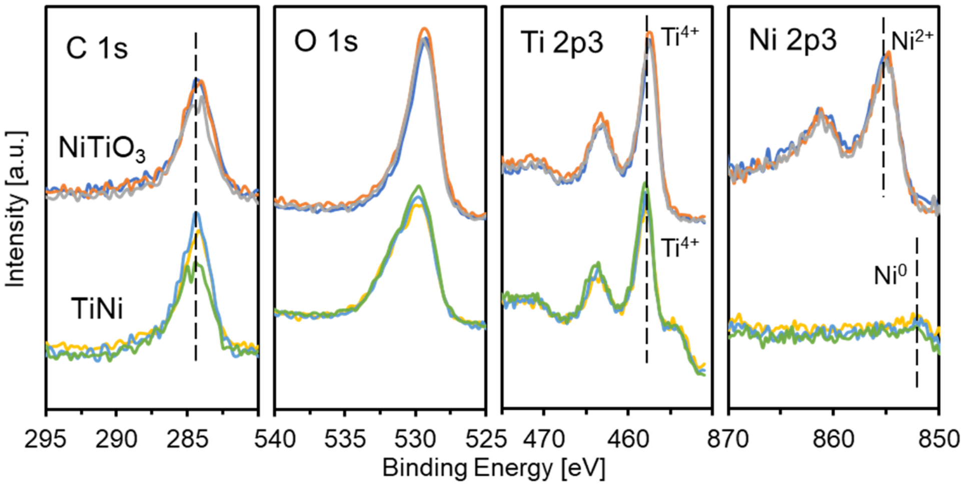

Figure 4. XPS spectra for $NiTiO_3$ (top) and the prepared TiNi (bottom). Each data was measured at three different positions, and each data is shown above by different color.

3.2. Catalytic Hydrogenation of 4-Nitrophenol

The morphology of the catalyst plays an important role for the catalytic activity. Currently, some core–shelled and hollow structures are extensively used in catalysis, showing unique and superior catalytic performance [40–42]. In this study, we evaluated the catalytic performance of the core–shelled TiNi in hydrogenation of 4-NP to 4-aminophnol (4-AP). $NaBH_4$ was used to catalyze the hydrogenation of 4-NP at 40–50 °C using the prepared TiNi, $NiTiO_3$, and TiO_2. The absorbance change in the reaction solution during the TiNi reaction is shown in Figure 5a. The absorbance at 315 nm to the production concentration of *p*-aminophenol increased, as the absorbance at 401 nm corresponding to the concentration of 4-NP decreased with reaction time, indicating the progress of the hydrogenation reaction. The concentration change in 4-NP during the reactions with catalysts TiNi, $NiTiO_3$, and TiO_2 is shown in Figure 5b. For $NiTiO_3$ and TiO_2 at 40 °C, little changes were observed in the concentrations, indicating that they had no catalytic abilities in the reaction system. For TiNi at 50 °C, the catalytic tests were conducted there times repeatedly with the identical catalyst powder in order to confirm the recyclability of the prepared TiNi powder. The concentration decreased rapidly with the reaction time and 100% conversion was obtained in 15–40 min. These results showed that the active species were not TiO_x and Ni (+4) but metallic Ni (0). The activities of 2nd and 3rd runs were higher than 1st one. This could be because the TiNi catalyst was more activated in the 2nd and 3rd runs due to the removal of surface TiO_x passivation during the hydrogenation reaction. The reaction rate constant of 0.14–0.31 min^{-1} was obtained from a plot of $\ln(C/C_0)$ versus time (Figure 5c), where C and C_0 represent the concentration of 4-NP at distinct and initial times, respectively. The rate constants of this study and previous studies with nickel-based catalysts are summarized in Table 2. Because the reaction conditions differed, a quantitative comparison was difficult. Our result was reasonably comparable with those obtained using the previously reported nickel-based catalysts. Particularly, the prepared TiNi exhibited a higher constant than the multicomponent alloy catalysts of AlCoCrFeNiV and CrMnFeCoNi under similar reaction conditions. Despite a limited amount of metallic Ni (0) exposed on the surface, as confirmed by XPS, the prepared TiNi exhibited promising catalytic performance. As the results of the previous works [43,44], heterogeneous hydrogenation of 4-NP to 4-AP by $NaBH_4$ proceeds in accordance with the Langmuir–Hinshelwood (LH) model. In the first step, the $NaBH_4$ is decomposed by hydrolysis, then the $B(OH)_4^-$ and active hydrogen (or, hydride) are formed. The active hydrogen diffuses to adsorb on the surface of active metals, such as gold and silver nanoparticles. 4-NP also diffuses to adsorb on the surface. Finally, the adsorbed active hydrogen reacts with 4-NP to yield the product 4-AP. The rate-determining step is given by the surface reaction of the adsorbed species. In our study, therefore, the surface-exposed Ni (0) was well-dispersed across the surface in the form of small nanoparticles, resulting in numerous active sites. The active sites could effectively work to promote the surface reaction to obtain the fast reaction rates. The XRD patterns of the used TiNi catalyst powder is shown in Figure 6. The identical XRD peaks with the fresh TiNi powder were observed and the result indicated that the prepared TiNi powder was stable without decomposition during the hydrogenation reactions.

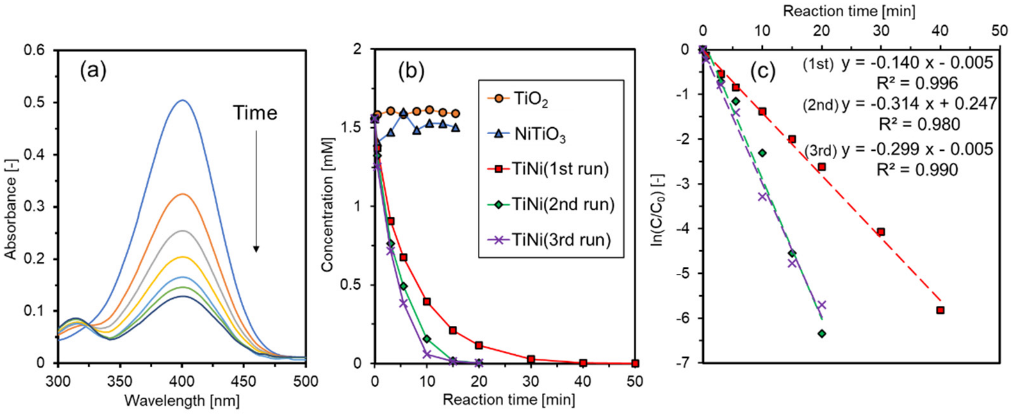

Figure 5. (**a**) Absorbance changes of 4-NP solutions with a reaction time for the prepared NiTi, (**b**) changes in 4-NP concentration (C) versus time for the TiNi at 50 °C, $NiTiO_3$ and TiO_2 at 40 °C, and (**c**) a plot of $\ln(C/C_0)$ versus time to acquire rate constants (k). For the prepared TiNi, the catalytic tests were repeated three times to examine the recyclability.

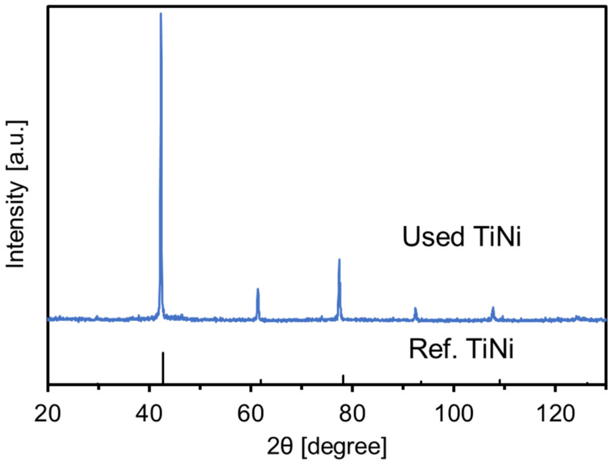

Figure 6. XRD patterns of the used TiNi catalyst powder.

Table 2. Comparison of rate constants (k) for 4-NP reduction.

Sample	Temp. [°C]	Reaction Conditions	k [min^{-1}]	Ref.
TiNi	50	4-NP (1.6 mM) $NaBH_4$ (47 mM) 10 mg-cat/9 mL	0.14–0.31	This study
Ni film	25	4-NP (0.1 mM) $NaBH_4$ (10 mM) 15 cm^2-cat/16 mL	0.09	[45]
$Co_{50}Ni_{50}$ film			0.15	
$Co_{25}Ni_{75}$ film			0.14	
p(MAc)-Ni	30	4-NP (10 mM) $NaBH_4$ (400 mM) 5 mg-cat(Ni)/50 mL	0.75	[46]
Ni-RGO	R.T.	4-NP (0.1 mM) $NaBH_4$ (30 mM) 10 mg-cat/104 mL	0.07	[47]
Ni NP			0.02	
SiO_2@C/Ni	R.T.	4-NP (0.2 mM) $NaBH_4$ (65 mM) 3 mg-cat/3.1 mL	2.19–3.06	[48]
AlCoCrFeNiV	53	4-NP (1.6 mM) $NaBH_4$ (47 mM) 10 mg-cat/9 mL	0.05	[49]
CrMnFeCoNi	50	4-NP (0.16 mM) $NaBH_4$ (60 mM) 10 mg-cat/9 mL	0.11	[35]

4. Conclusions

Intermetallic compound TiNi powder passivated by TiO_x shell was successfully prepared from $NiTiO_3$ by reducing it at 650 °C in a molten LiCl-CaH_2 system. XRD, SEM-/TEM-EDX, and XPS analyses demonstrated that the obtained TiNi possessed a core–shelled structure, such as the core of intermetallic compound TiNi and the shell of TiO_x-rich composition with a scarce amount of metallic Ni. The scarce metallic Ni demonstrated promising high catalytic performance in the hydrogenation of 4-NP because of the good dispersion of active Ni species on the surface.

Supplementary Materials: The following supporting information can be downloaded at: https://www.mdpi.com/article/10.3390/ma15238536/s1, Figure S1. SEM images of commercial $NiTiO_3$. Figure S2. SEM images of TiNi prepared by reducing $NiTiO_3$ via CaH_2 in molten LiCl at 800 °C. Figure S3. TEM images and the EDX result of the prepared TiNi. Figure S4. XPS spectra measured in a wide-scan mode of $NiTiO_3$ and the prepared TiNi.

Author Contributions: Conceptualization, Y.K.; methodology, Y.K., S.Y.; validation, Y.K.; formal analysis, Y.K.; investigation, Y.K., R.S.; resources, Y.K., R.S.; data curation, Y.K., S.Y.; writing—original draft preparation, Y.K.; writing—review and editing, Y.K., S.Y., R.S.; visualization, Y.K.; supervision, Y.K.; project administration, Y.K.; funding acquisition, Y.K., R.S. All authors have read and agreed to the published version of the manuscript.

Funding: This research was funded by Japan Society for the Promotion of Science (JSPS), grant number 21K14465.

Institutional Review Board Statement: Not applicable.

Informed Consent Statement: Not applicable.

Data Availability Statement: Not applicable.

Conflicts of Interest: The authors declare no conflict of interest.

References

1. Bansiddhi, A.; Sargeant, T.D.; Stupp, S.I.; Dunand, D.C. Porous NiTi for bone implants: A review. *Acta Biomater.* **2008**, *4*, 773–782. [CrossRef] [PubMed]
2. Plotino, G.; Grande, N.M.; Cordaro, M.; Testarelli, L.; Gambarini, G. A Review of Cyclic Fatigue Testing of Nickel-Titanium Rotary Instruments. *J. Endod.* **2009**, *35*, 1469–1476. [CrossRef] [PubMed]
3. Shen, Y.; Zhou, H.; Zheng, Y.; Peng, B.; Haapasalo, M. Current Challenges and Concepts of the Thermomechanical Treatment of Nickel-Titanium Instruments. *J. Endod.* **2013**, *39*, 163–172. [CrossRef] [PubMed]
4. Sharma, N.; Raj, T.; Jangra, K.K. Applications of Nickel-Titanium Alloy. *J. Eng. Technol.* **2015**, *5*, 1–7. [CrossRef]
5. Zhang, N.; Khosrovabadi, P.B.; Lindenhovius, J.H.; Kolster, B.H. TiNi shape memory alloys prepared by normal sintering. *Mater. Sci. Eng. A* **1992**, *150*, 263–270. [CrossRef]
6. Hey, J.C.; Jardine, A.P. Shape memory TiNi synthesis from elemental powders. *Mater. Sci. Eng. A* **1994**, *188*, 291–300. [CrossRef]
7. Inoue, H.; Ishio, M.; Takasugi, T. Texture of TiNi shape memory alloy sheets produced by roll-bonding and solid phase reaction from elementary, metals. *Acta Mater.* **2003**, *51*, 6373–6383. [CrossRef]
8. Zhu, S.L.; Yang, X.J.; Hu, F.; Deng, S.H.; Cui, Z.D. Processing of porous TiNi shape memory alloy from elemental powders by Ar-sintering. *Mater. Lett.* **2004**, *58*, 2369–2373. [CrossRef]
9. Ergin, N.; Ozdemir, O. An Investigation on TiNi Intermetallic Produced by Electric Current Activated Sintering. *Acta Phys. Pol.* **2013**, *123*, 248–249. [CrossRef]
10. Barbat, N.; Zangeneh-Madar, K. Fabrication and characterization of NiTi shape memory alloy synthesized by Ni electroless plating of titanium powder. *Adv. Powder Technol.* **2018**, *29*, 1005–1013. [CrossRef]
11. Li, B.Y.; Rong, L.J.; Li, Y.Y.; Gjunter, V.E. Synthesis of porous Ni–Ti shape-memory alloys by self-propagating high-temperature synthesis: Reaction mechanism and anisotropy in pore structure. *Acta Mater.* **2000**, *48*, 3895–3904. [CrossRef]
12. Yeh, C.L.; Sung, W.Y. Synthesis of NiTi intermetallics by self-propagating combustion. *J. Alloys Compd.* **2004**, *376*, 79–88. [CrossRef]
13. Khodorenko, V.N.; Guenther, V.E.; Soldatova, M.I. Influence of heat treatment on shape memory effect in porous titanium nickel synthesized by the SHS process. *Russ. Phys. J.* **2011**, *53*, 1024–1034. [CrossRef]
14. Bassani, P.; Panseri, S.; Ruffini, A.; Montesi, M.; Ghetti, M.; Zanotti, C.; Tampieri, A.; Tuissi, A. Porous NiTi shape memory alloys produced by SHS: Microstructure and biocompatibility in comparison with Ti_2Ni and $TiNi_3$. *J. Mater. Sci. Mater. Med.* **2014**, *25*, 2277–2285. [CrossRef] [PubMed]
15. Yasenchuk, Y.F.; Artyukhova, N.V.; Novikov, V.A.; Gyunter, V.E. Participation of Gases in the Surface Formation during Self-Propagating High-Temperature Synthesis of Porous Nickel Titanium. *Tech. Phys. Lett.* **2014**, *40*, 697–700. [CrossRef]
16. Novák, P.; Veselý, T.; Marek, I.; Dvořák, P.; Vojtěch, V.; Salvetr, P.; Karlík, M.; Haušild, P.; Kopeček, J. Effect of Particle Size of Titanium and Nickel on the Synthesis of NiTi by TE-SHS. *Metall. Mater. Trans. B* **2016**, *47*, 932–938. [CrossRef]
17. Gunther, V.; Yasenchuk, Y.; Chekalkin, T.; Marchenko, E.; Gunther, S.; Baigonakova, G.; Hodorenko, V.; Kang, J.; Weiss, S.; Obrosov, A. Formation of pores and amorphous-nanocrystalline phases in porous TiNi alloys made by self-propagating high-temperature synthesis (SHS). *Adv. Powder Technol.* **2019**, *30*, 673–680. [CrossRef]
18. Li, Y.; Rong, L.; Li, Y. Pore characteristics of porous NiTi alloy fabricated by combustion synthesis. *J. Alloys Compd.* **2001**, *325*, 259–262. [CrossRef]
19. Chu, C.L.; Chung, C.Y.; Lin, P.H.; Wang, S.D. Fabrication of porous NiTi shape memory alloy for hard tissue implants by combustion synthesis. *Mater. Sci. Eng. A* **2004**, *366*, 114–119. [CrossRef]
20. He, J.L.; Won, K.W.; Chang, J.T. TiNi thin films prepared by cathodic arc plasma ion plating. *Thin Solid Film.* **2000**, *359*, 46–54. [CrossRef]
21. Gao, F.; Wang, H.M. Dry sliding wear property of a laser melting/deposited Ti_2Ni/TiNi intermetallic alloy. *Intermetallics* **2008**, *16*, 202–208. [CrossRef]
22. Wei, C.; Xue, F.; Jiehe, S. Preparation of multi-walled carbon nanotube-reinforced TiNi matrix composites from elemental powders by spark plasma sintering. *Rare Metals* **2012**, *31*, 48–50.
23. Shi, Q.; Zhang, Y.; Tan, C.; Mao, X.; Khanlari, K.; Liu, X. Preparation of Ni–Ti composite powder using radio frequency plasma spheroidization and its laser powder bed fusion densification. *Intermetallics* **2021**, *136*, 107273. [CrossRef]
24. Kobayashi, Y.; Yamaoka, S.; Yamaguchi, S.; Hanada, N.; Tada, S.; Kikuchi, R. Low-temperature chemical synthesis of intermetallic TiFe nanoparticles for hydrogen absorption. *Int. J. Hydrog. Energy* **2021**, *46*, 22611–22617. [CrossRef]
25. Kobayashi, Y.; Teah, H.Y.; Hanada, N. Chemical synthesis of unique intermetallic TiFe nanostructures originating from the morphology of oxide precursors. *Nanoscale Adv.* **2021**, *3*, 5284–5291. [CrossRef] [PubMed]
26. Itahara, H.; Simanullang, W.F.; Takahashi, N.; Kosaka, S.; Furukawa, S. Na-Melt Synthesis of Fine Ni_3Si Powders as a Hydrogenation Catalyst. *Inorg. Chem.* **2019**, *58*, 5406–5409. [CrossRef]
27. Fouilloux, P. The nature of raney nickel, its adsorbed hydrogen and its catalytic activity for hydrogenation reactions (review). *Appl. Catal.* **1983**, *8*, 1–42. [CrossRef]
28. Alonso, F.; Riente, P.; Yus, M. Nickel nanoparticles in hydrogen transfer reactions. *Acc. Chem. Res.* **2011**, *44*, 379–391. [CrossRef]
29. De, S.; Zhang, J.; Luque, R.; Yan, N. Ni-based bimetallic heterogeneous catalysts for energy and environmental applications. *Energy Environ. Sci.* **2016**, *9*, 3314–3347. [CrossRef]
30. Zhou, C.; Zhang, J.; Bowman, R.C.; Fang, Z.Z. Roles of Ti-Based Catalysts on Magnesium Hydride and Its Hydrogen Storage Properties. *Inorganics* **2021**, *9*, 36. [CrossRef]

31. Khan, M.M.; Saadah, N.H.; Khan, M.E.; Harunsani, M.H.; Tan, A.L.; Cho, M.H. Potentials of *Costus woodsonii* leaf extract in producing narrow band gap ZnO nanoparticles. *Mater. Sci. Semicond. Process* **2019**, *91*, 194–200. [CrossRef]
32. Sharwani, A.A.; Narayanan, K.B.; Khan, M.E.; Han, S.S. Photocatalytic degradation activity of goji berry extract synthesized silver-loaded mesoporous zinc oxide (Ag@ZnO) nanocomposites under simulated solar light irradiation. *Sci. Rep.* **2022**, *12*, 10017. [CrossRef] [PubMed]
33. Kobayashi, Y. Synthesis of Porous Ni_3Al Intermetallic Nano-compounds in a Molten LiCl with Assistance of CaH_2 as a Structure-controlling Agent. *Chem. Lett.* **2019**, *48*, 1496–1499. [CrossRef]
34. Garay, J.E.; Anselmi-Tamburini, U.; Munir, Z.A. Enhanced growth of intermetallic phases in the Ni–Ti system by current effects. *Acta Mater.* **2003**, *51*, 4487–4495. [CrossRef]
35. Peng, H.; Xie, Y.; Xie, Z.; Wu, Y.; Zhu, W.; Liang, S.; Wang, L. Large-scale and facile synthesis of a porous high entropy alloy CrMnFeCoNi as an efficient catalyst. *J. Mater. Chem. A* **2020**, *8*, 18318–18326. [CrossRef]
36. Kobayashi, Y.; Kanasaki, R.; Nozaki, T.; Shoji, R.; Sato, K. Improving Effect of MnO_2 Addition on TiO_2-Photocatalytic Removal of Lead Ion from Water. *J. Water Environ. Technol.* **2017**, *15*, 35–42. [CrossRef]
37. Devi, T.G.; Kannan, M.P. X-ray Diffraction (XRD) Studies on the Chemical States of Some Metal Species in Cellulosic Chars and the Ellingham Diagrams. *Energy Fuels* **2007**, *21*, 596–601. [CrossRef]
38. Hanawa, T. A comprehensive review of techniques for biofunctionalization of titanium. *J. Periodontal Implant Sci.* **2011**, *41*, 263–272. [CrossRef]
39. Grosvenor, A.P.; Biesinger, M.C.; Smart RS, C.; McIntyre, N.S. New interpretations of XPS spectra of nickel metal and oxides. *Surf. Sci.* **2006**, *600*, 1771–1779. [CrossRef]
40. Zhao, K.; Qi, J.; Zhao, S.; Tang, H.; Yin, H.; Zong, L.; Chang, L.; Gao, Y.; Yu, R.; Tang, Z. Multiple Au cores in CeO_2 hollow spheres for the superior catalytic reduction of *p*-nitrophenol. *Chin. J. Catal.* **2015**, *36*, 261–267. [CrossRef]
41. You, F.; Wan, J.; Qi, J.; Mao, D.; Yang, N.; Zhang, Q.; Gu, L.; Wang, D. Lattice Distortion in Hollow Multi-Shelled Structures for Efficient Visible-Light CO_2 Reduction with a SnS_2/SnO_2 Junction. *Angew. Chem. Int. Ed.* **2020**, *59*, 721–724. [CrossRef] [PubMed]
42. Wang, Z.; Qi, J.; Yang, N.; Yu, R.; Wang, D. Core–shell nano/microstructures for heterogeneous tandem catalysis. *Mater. Chem. Front.* **2021**, *5*, 1126–1139. [CrossRef]
43. Wunder, S.; Polzer, F.; Lu, Y.; Mei, Y.; Ballauff, M. Kinetic Analysis of Catalytic Reduction of 4-Nitrophenol by Metallic Nanoparticles Immobilized in Spherical Polyelectrolyte Brushes. *J. Phys. Chem. C* **2010**, *114*, 8814. [CrossRef]
44. Zhao, P.; Feng, X.; Huang, D.; Yang, G.; Astruc, D. Basic concepts and recent advances in nitrophenol reduction by gold- and other transition metal nanoparticles. *Coord. Chem. Rev.* **2015**, *287*, 114. [CrossRef]
45. Li, H.; Liao, J.; Du, Y.; You, T.; Liao, W.; Wen, L. Magnetic-field-induced deposition to fabricate multifunctional nanostructured Co, Ni, and CoNi alloy films as catalysts, ferromagnetic and superhydrophobic materials. *Chem. Commun.* **2013**, *49*, 1768–1770. [CrossRef]
46. Ajmal, M.; Siddiq, M.; Al-Lohedan, H.; Sahiner, N. Highly versatile p(MAc)–M (M: Cu, Co, Ni) microgel composite catalyst for individual and simultaneous catalytic reduction of nitro compounds and dyes. *RSC Adv.* **2014**, *4*, 59562–59570. [CrossRef]
47. Qiu, H.; Qiu, F.; Han, X.; Li, J.; Yang, J. Microwave-irradiated preparation of reduced graphene oxide-Ninanostructures and their enhanced performance for catalyticreduction of 4-nitrophenol. *Appl. Surf. Sci.* **2017**, *407*, 509–517. [CrossRef]
48. Yang, X.; Wang, Z.; Shang, Y.; Zhang, Y.; Lou, Q.; Li, B.; Xu, J. Well dispersive Ni nanoparticles embedded in core-shell supports as efficient catalysts for 4-nitrophenol reduction. *J. Nanopart. Res.* **2019**, *21*, 120. [CrossRef]
49. Kobayashi, Y.; Suzuki, D.; Yokoyama, S.; Shoji, R. Molten salt synthesis of high-entropy alloy AlCoCrFeNiV nanoparticles for the catalytic hydrogenation of p-nitrophenol by $NaBH_4$. *Int. J. Hydrog. Energy* **2022**, *47*, 3722–3732. [CrossRef]